Defining quality measures for high-order planar triangles and curved mesh generation

Xevi Roca[1,2], Abel Gargallo-Peiró[1] and Josep Sarrate[1]

[1] Laboratori de Càlcul Numèric (LaCàN),
Universitat Politècnica de Catalunya, Barcelona 08034, Spain
{xevi.roca,abel.gargallo,jose.sarrate}@upc.edu
[2] Department of Aeronautics and Astronautics
Massachusetts Institute of Technology, Cambridge, MA 02139, USA
xeviroca@mit.edu

Summary. We present a technique to extend any Jacobian based quality measure for linear elements to high-order isoparametric planar triangles of any interpolation degree. The extended quality measure is obtained as the inverse of the distortion of the high-order element with respect to an ideal element. To measure the high-order distortion, we integrate on the curved element the inverse of the Jacobian based quality measure. Thus, we can proof that if the Jacobian based quality is invariant under a particular affine mapping, then the resulting quality measure is also invariant under that mapping. In addition, we check that the quality measure detects non-valid and low-quality high-order elements. Finally, we present and test an approach to generate curved meshes by minimizing the high-order distortion measure of the elements.

Key words: High-order quality, high-order mesh generation, mesh optimization, curved elements

1 Introduction

In the last decades several computational methods have been widely used to solve partial differential equations (PDE) in applied sciences and engineering. Some of these methods allow the use of unstructured meshes, such as the finite element method (FEM), the finite volume method (FVM), and the discontinuous Galerkin method (DG). The unstructured methods have been proven to be very successful to solve PDE in complex domains (geometry flexibility). To solve a PDE with these methods, an unstructured mesh of the domain is generated. Then, a linear system is created by assembling the contributions of each mesh element to the system matrix. These contributions can be computed by integrating directly in the physical element or by changing the variable and integrating in a reference element.

To apply the reference element approach, it is required to use a differentiable, invertible and smooth mapping (diffeomorphism) from the reference element to the mesh element. Hence, the mapping has to be expressed by means of differentiable functions and the mesh elements have to be valid (non-folded) and present high-quality (regular shape). If one element is invalid then the determinant of the mapping Jacobian presents non-positive values. These non-positive determinant values invalidate the change of variable, and therefore, the obtained solution. Moreover, if one element has low quality then the element is distorted respect a regular element. Thus, the approximation accuracy is degraded and the solution may be polluted by the introduced error [1]. In summary, quality measures have to be used to assess the validity and quality of a given mesh.

Quality measures also have an alternative and significant application. They allow the use of optimization based techniques to repair non-valid meshes (untangle) and to improve the mesh quality (smooth) by maximizing the quality of the mesh elements. This technique allows the generation of high-order meshes with a posteriori approach [2, 3, 4, 5, 6, 7]. That is, it allows the generation of meshes that might contain inverted or low-quality elements, and then untangle and smooth them a posteriori to ensure and enhance the mesh quality. Specifically, a high-order mesh can be obtained by generating first a linear mesh. Second, the linear mesh is converted to a high-order mesh by adding additional nodes and by curving the boundary elements. Finally, the converted mesh is untangled and smoothed to remove the non-valid (folded) and low-quality (distorted) elements. However, the application of this approach together with a mesh quality optimization has been hampered by the absence of quality measures for high-order iso-parametric elements with degree superior than two. Note that the capability of generating valid high-order meshes is of the major importance for the high-order methods community.

The main contribution of this work is to present a technique that allows extending any Jacobian based quality measure for linear elements to high-order iso-parametric planar triangles of any interpolation degree. The proposed approach is compared with other related work in Section 2. Similarly to the linear elements technique, we measure the deviation of the physical element respect an ideal element. Specifically, we integrate the selected Jacobian based distortion measure in the curved element. Then, the quality measure for high-order elements is defined as the inverse of this distortion measure. The resulting quality inherits some of the properties of the original linear quality measures, Section 3. We also check that the proposed measure detects non-valid and low-quality elements for different initial Jacobian based quality measures, Section 4. To assess the applicability of the proposed measures, we overview a technique to optimize high-order meshes by minimizing the proposed distortion measure, Section 5. Finally, we apply this optimization technique to untangle and smooth several high-order triangular meshes, Section 6.

2 Related work

In this work we propose an extension of quality measures for linear elements that allows determining the quality of iso-parametric elements of any interpolation degree. There are several previous works that determine the distortion or the quality of non-linear iso-parametric elements but only for quadratic degree [8, 9, 10, 11, 12, 13]. We would like to highlight that we share a similar formulation to the one proposed before by Branets and Carey in [10]. However, they extend only one distortion measure to quadratic elements, while we can extend any Jacobian based distortion measure to any interpolation degree. A different approach to extend Jacobian based disortion measures was previously proposed by Knupp [14]. The main difference is that we propose to integrate the distortion measure on the curved element, instead of computing the minimum, maximum or the mean on a set of sampling points. In addition, we also present numerical tests and mesh optimizations beyond the quadratic case.

The proposed extension of quality measures also allows the detection of non-positive values of the Jacobian determinant of the reference mapping for any interpolation degree. If the quality is strictly positive, we can ensure that the reference mapping is a local diffeomorphism. Other techniques to detect non-positive Jacobian determinants have been proposed before for B-spline based mappings [2, 3, 4, 5, 6] and quadratic iso-parametric elements [15, 16, 17]. Note that checking that the Jacobian determinant is strictly positive is not a guarantee for the global invertibility of the reference mapping for non-linear elements. That is, it is also required to check that the image of the reference mapping is simply connected [18]. In this work we do not study the conditions on the coordinates of the element nodes that ensure simply connected images, and therefore, global invertibility. It is important to point out that these conditions have been studied only in 2D for quadratic iso-parametric elements in [19, 20].

Finally, the proposed measures allow untangling and smoothing non-valid and low-quality high-order meshes. The optimization technique is a generalization of the methods for linear elements of Knupp [21] and Escobar *et al.* [22]. A similar optimization method has been presented previously by Branets and Carey for quadratic elements [10]. The main application of the untangling and smoothing method is to generate curved meshes by means of the named a posteriori approach. We have to remark that the a posteriori approach has been previously used with success by Shephard and co-workers for B-spline mappings [2, 3, 4, 5, 6] (instead of iso-parametric elements), and by Persson and Peraire by means of a nonlinear elasticity problem [7] (instead of optimizing a quality measure).

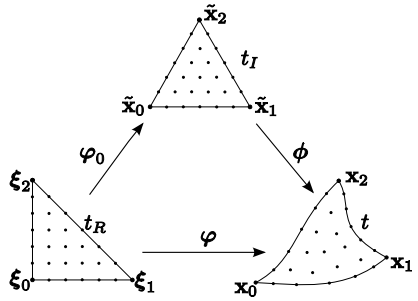

Fig. 1. Mappings between the reference, the ideal and the physical elements.

3 Quality measures for high-order triangles

In order to determine the quality of a high-order triangular element t, we generalize the Jacobian based quality measures for linear elements [23, 24], Section 3.1. To this end, we consider a mapping $\boldsymbol{\phi}$ from the ideal element t_I to the physical element t. To determine this mapping, we consider two high-order isoparametric mappings (Section 3.1), $\boldsymbol{\varphi}$ and $\boldsymbol{\varphi}_0$, from a reference element t_R to t and t_I, respectively. Figure 1 presents the generalized diagram of mappings between the reference, the ideal and the physical high-order elements. This setting allows extending a Jacobian based distortion measure to high-order elements, Section 3.2. The proposed high-order quality measure inherits some properties of the initial Jacobian based quality measure, Section 3.3. In addition, the proposed definitions allow detecting invalid and low quality elements for different initial Jacobian based quality measures, Section 4.

3.1 Preliminaries

Jacobian based quality metrics

For linear elements, the three mappings presented in Figure 1 are affine. In particular, the mapping between the reference and the ideal element is:

$$\begin{aligned} \boldsymbol{\varphi}_0 : \; & t_R \longrightarrow t_I \\ & \boldsymbol{\xi} \longmapsto \tilde{\mathbf{x}} = \mathbf{W}\boldsymbol{\xi} + \tilde{\mathbf{x}}_0, \end{aligned} \tag{1}$$

where

$$\mathbf{W} = (\tilde{\mathbf{x}}_1 - \tilde{\mathbf{x}}_0 \quad \tilde{\mathbf{x}}_2 - \tilde{\mathbf{x}}_0) = \begin{pmatrix} \tilde{x}_1 - \tilde{x}_0 & \tilde{x}_2 - \tilde{x}_0 \\ \tilde{y}_1 - \tilde{y}_0 & \tilde{y}_2 - \tilde{y}_0 \end{pmatrix} \tag{2}$$

is a constant matrix. The ideal element is chosen to be a valid and properly oriented element. Thus, $\boldsymbol{\varphi}_0^{-1}$ exists and is affine, since $\mathbf{W}$ is not singular. Similarly, the mapping between the reference and the physical triangle is defined as:

$$\begin{aligned} \boldsymbol{\varphi} : \; & t_R \longrightarrow t \\ & \boldsymbol{\xi} \longmapsto \mathbf{x} = \mathbf{A}\boldsymbol{\xi} + \mathbf{x}_0, \end{aligned} \tag{3}$$

Name	Distortion measure $\eta(\mathbf{S})$
Shape measure	$\eta(\mathbf{S}) = \frac{\|\|\mathbf{S}\|\|^2}{d \cdot \sigma(\mathbf{S})^{2/d}}$
Oddy et al. measure	$\eta(\mathbf{S}) = \frac{3}{d}\sigma^{-4/d}(\mathbf{S}) \left(\|\|\mathbf{S}^T\mathbf{S}\|\|^2 - \frac{1}{3}\|\|\mathbf{S}\|\|^4 \right)$
Condition number	$\eta(\mathbf{S}) = \frac{1}{2}\|\|\mathbf{S}\|\| \cdot \|\|\mathbf{S}^{-1}\|\|$

Table 1. Algebraic distortion measures for linear elements

where

$$\mathbf{A} = (\mathbf{x}_1 - \mathbf{x}_0 \quad \mathbf{x}_2 - \mathbf{x}_0).$$

Hence, $\boldsymbol{\varphi}$ is also an affine mapping with a constant Jacobian matrix $\mathbf{A}$. Finally, a mapping between the ideal and the physical element is determined by

$$\boldsymbol{\phi} = \boldsymbol{\varphi} \circ \boldsymbol{\varphi}_0^{-1}. \tag{4}$$

Note that $\boldsymbol{\phi}$ is also an affine mapping, since $\boldsymbol{\varphi}_0^{-1}$ and $\boldsymbol{\varphi}$ are so. Moreover, the Jacobian of $\boldsymbol{\phi}$ is constant and can be written as

$$\mathbf{S} := \mathbf{D}\boldsymbol{\phi} = \mathbf{A} \cdot \mathbf{W}^{-1}. \tag{5}$$

For linear elements it is usual to define a distortion measure in terms of the Jacobian matrix (5). These distortion measures, herein denoted by $\eta(\mathbf{S})$, quantify a specific type of distortion of the physical element in a range scale $[1, \infty)$. In addition, the quality measures of the physical elements are defined as the inverse of these distortion measures:

$$q(\mathbf{S}) = \frac{1}{\eta(\mathbf{S})}. \tag{6}$$

Several distortion measures for linear triangles have been proposed in literature, see [23]. In Table 1 we present three distortion measures that we use to test the proposed high-order quality measure, Section 4. In Table 1, parameter d is the number of spatial dimensions, $\sigma(\mathbf{S})$ is a function of the determinant of $\mathbf{S}$, and $||\mathbf{S}|| = \sqrt{\text{tr}(\mathbf{S}^t\mathbf{S})}$ is its Frobenius norm. In general $\sigma(\mathbf{S}) := \det \mathbf{S}$. However, to compute the quality of an element we set $\sigma(\mathbf{S}) = \frac{1}{2}(\det \mathbf{S} + |\det \mathbf{S}|)$ to assign a null quality to inverted elements ($\det \mathbf{S} < 0$).

Nodal high-order triangles

Let t be a nodal high-order element of order p determined by n_p nodes with coordinates $\mathbf{x}_i \in \mathbb{R}^d$, for $i = 1, \ldots, n_p$. Given a reference element t_R with nodes $\boldsymbol{\xi}_j \in \mathbb{R}^d$, $j = 1, \ldots, n_p$, we consider the basis $\{N_i\}_{i=1,\ldots,n_p}$ of nodal shape functions (Lagrange interpolation) of order p. In this basis, the high-order isoparametric mapping from t_R to t can be expressed as:

$$\begin{aligned} \boldsymbol{\varphi} : t_R \subset \mathbb{R}^d &\longrightarrow t \subset \mathbb{R}^d \\ \boldsymbol{\xi} &\longmapsto \mathbf{x} = \boldsymbol{\varphi}(\boldsymbol{\xi}; \mathbf{x}_1, \ldots, \mathbf{x}_{n_p}) = \sum_{i=1}^{n_p} \mathbf{x}_i N_i(\boldsymbol{\xi}), \end{aligned} \tag{7}$$

where $\boldsymbol{\xi} = (\xi^1, \ldots, \xi^d)^T$ and $\mathbf{x} = (x^1, \ldots, x^d)^T$. Note that the shape functions $\{N_i\}_{i=1,\ldots,n_p}$ depend on the selection of $\boldsymbol{\xi}_j$, for $j = 1, \ldots, n_p$. In addition, they form a partition of the unity on t_R, and hold that $N_i(\boldsymbol{\xi}_j) = \delta_{ij}$, for $i, j = 1, \ldots, n_p$.

In this paper we focus on nodal high-order triangular elements of order p. Hence, the number of nodes n_p is $\frac{(p+1)(p+2)}{2}$, and the number of spatial dimensions d is 2. For this 2-dimensional case, the Jacobian of the isoparametric mapping (7) is:

$$\mathbf{D}\boldsymbol{\varphi}(\boldsymbol{\xi}; \mathbf{x}_1, \ldots, \mathbf{x}_{n_p}) = \begin{pmatrix} \displaystyle\sum_{i=1}^{n_p} x_i^1 \frac{\partial N_i}{\partial \xi^1}(\boldsymbol{\xi}) & \displaystyle\sum_{i=1}^{n_p} x_i^1 \frac{\partial N_i}{\partial \xi^2}(\boldsymbol{\xi}) \\ \displaystyle\sum_{i=1}^{n_p} x_i^2 \frac{\partial N_i}{\partial \xi^1}(\boldsymbol{\xi}) & \displaystyle\sum_{i=1}^{n_p} x_i^2 \frac{\partial N_i}{\partial \xi^2}(\boldsymbol{\xi}) \end{pmatrix}.$$

3.2 Definitions

To define the high-order distortion measure of the physical element, we have to select first the equilateral ideal element t_I and a distribution of points. Herein, we choose a straight-sided triangle as the ideal element. In addition, we map the chosen distribution on the reference element (*e.g.* equi-distributed or Fekete points) to determine the distribution on the ideal element. Note that the mapping $\boldsymbol{\varphi}_0$ is affine and its Jacobian matrix is given by equation (2). However, the mapping $\boldsymbol{\varphi}$ between the reference and the physical element, see Equation (7), can be not affine. Hence, $\boldsymbol{\phi} = \boldsymbol{\varphi} \circ \boldsymbol{\varphi}_0^{-1}$ is in general not affine, and the Jacobian matrix is not constant. The expression of the Jacobian is:

$$\begin{aligned} \mathbf{D}\boldsymbol{\phi}(\tilde{\mathbf{x}}; \mathbf{x}_1, \ldots, \mathbf{x}_{n_p}) &= \mathbf{D}(\boldsymbol{\varphi}(\cdot; \mathbf{x}_1, \ldots, \mathbf{x}_{n_p}) \circ \boldsymbol{\varphi}_0^{-1})(\tilde{\mathbf{x}}) \\ &= \mathbf{D}\boldsymbol{\varphi}(\boldsymbol{\varphi}_0^{-1}(\tilde{\mathbf{x}}); \mathbf{x}_1, \ldots, \mathbf{x}_{n_p}) \cdot \mathbf{D}\boldsymbol{\varphi}_0^{-1}(\tilde{\mathbf{x}}) \\ &= \mathbf{D}\boldsymbol{\varphi}(\boldsymbol{\varphi}_0^{-1}(\tilde{\mathbf{x}}); \mathbf{x}_1, \ldots, \mathbf{x}_{n_p}) \cdot \mathbf{W}^{-1}, \end{aligned} \tag{8}$$

where $\tilde{\mathbf{x}}$ is a point on the ideal triangle. Note that, according to (8), the local variation between the ideal and the physical triangles depends on $\tilde{\mathbf{x}}$ and also on the physical configuration of the high-order element $\mathbf{x}_1, \ldots, \mathbf{x}_{n_p}$.

Similar to the linear element case, we want to define a distortion measure based on the the Jacobian matrix of $\boldsymbol{\phi}$, see Equation (6). However, we cannot apply directly this approach because the Jacobian is not constant. Nevertheless, the Jacobian allows measuring the local deviation between the ideal and the physical element. Thus, we can obtain an elemental distortion measure by integrating the Jacobian based distortion measure on the whole physical element.

Definition 1. *The **high-order distortion measure** for a high-order element with nodes* $\mathbf{x}_1, \ldots, \mathbf{x}_{n_p}$ *is*

$$\hat{\eta}_r(\mathbf{x}_1, \ldots, \mathbf{x}_{n_p}) := \left(\frac{1}{|t|} \int_t \eta^r(\mathbf{D}\boldsymbol{\phi}(\boldsymbol{\phi}^{-1}(\mathbf{x}); \mathbf{x}_1, \ldots, \mathbf{x}_{n_p}))\ d\mathbf{x} \right)^{\frac{1}{r}}, \tag{9}$$

where η *is a distortion measure for linear elements based on the Jacobian matrix (see Table 1),* $|t|$ *is the area of the physical triangle, and* r *is a real number greater or equal to one.*

Remark 1. Taking into account the change of variable determined by the isoparametric mapping $\boldsymbol{\varphi}$ and expression (8), we compute the distortion as:

$$\hat{\eta}_r(\mathbf{x}_1, \ldots, \mathbf{x}_{n_p}) = \left(\frac{1}{|t|} \int_{t_R} \eta^r \left(\mathbf{D}\boldsymbol{\varphi}(\boldsymbol{\xi}) \cdot \mathbf{W}^{-1} \right) \cdot |\det\ \mathbf{D}\boldsymbol{\varphi}(\boldsymbol{\xi})|\ \mathrm{d}\boldsymbol{\xi} \right)^{\frac{1}{r}}.$$

In practical applications, we approximate the value of this integral with the symmetrical numerical quadrature for high-order triangles proposed in [25].

Definition 2. *The **high-order quality measure** for a high-order element with nodes* $\mathbf{x}_1, \ldots, \mathbf{x}_{n_p}$ *is*

$$\hat{q}_r(\mathbf{x}_1, \ldots, \mathbf{x}_{n_p}) := \frac{1}{\hat{\eta}_r(\mathbf{x}_1, \ldots, \mathbf{x}_{n_p})}. \tag{10}$$

3.3 Properties

The proposed high-order distortion and quality measures, Definitions 1 and 2, present several properties. First, it is straightforward to prove that the linear case is just a particular case of these generalizations. That is, $\hat{\eta}_r(\mathbf{x}_1, \mathbf{x}_2, \mathbf{x}_3) = \eta(\mathbf{S}(\mathbf{x}_1, \mathbf{x}_2, \mathbf{x}_3))$ and $\hat{q}_r(\mathbf{x}_1, \mathbf{x}_2, \mathbf{x}_3) = q(\mathbf{S}(\mathbf{x}_1, \mathbf{x}_2, \mathbf{x}_3))$. Second, $\hat{\eta}_r$ and $\hat{q}_r$ maintain the image range of their respective linear distortion and quality measures. In particular, let q be a quality measure for linear elements with image range $[0, 1]$. Then, $\hat{q}_r$ is a quality measure for high-order elements with image range $[0, 1]$. Finally, we prove that $\hat{\eta}_r$ and $\hat{q}_r$ inherit the geometric properties of the Jacobian based distortion measure η.

Proposition 1. *If* η *is invariant under an affine mapping* ψ*, then* $\hat{\eta}_r$ *is also invariant under* ψ*.*

Proof. The affine mapping ψ can be written as $\psi(\mathbf{x}) := \mathbf{A}\mathbf{x} + \mathbf{b}$, where $\mathbf{A}$ is the linear mapping, and $\mathbf{b}$ is the translation vector. Thus, the transformation of the high-order element by the mapping ψ is the isoparametric mapping for the points $\psi(\mathbf{x}_i),\ i = 1, \ldots, n_p$:

$$\begin{aligned}
\psi(\boldsymbol{\phi}(\tilde{\mathbf{x}};\mathbf{x}_1,\dots,\mathbf{x}_{n_p})) &= \mathbf{A}\cdot\boldsymbol{\phi}(\tilde{\mathbf{x}};\mathbf{x}_1,\dots,\mathbf{x}_{n_p})+\mathbf{b}\\
&\overset{\mathbf{A}\text{ is linear}}{=} \sum_{i=1}^{n_p}\mathbf{A}\mathbf{x}_i N_i(\boldsymbol{\varphi}_0^{-1}(\tilde{\mathbf{x}}))+\mathbf{b}\\
&\overset{\text{Partit. unity}}{=} \sum_{i=1}^{n_p}\mathbf{A}\mathbf{x}_i N_i(\boldsymbol{\varphi}_0^{-1}(\tilde{\mathbf{x}}))+\sum_{i=1}^{n_p}\mathbf{b}N_i(\boldsymbol{\varphi}_0^{-1}(\tilde{\mathbf{x}}))\\
&= \sum_{i=1}^{n_p}(\mathbf{A}\mathbf{x}_i+\mathbf{b})N_i(\boldsymbol{\varphi}_0^{-1}(\tilde{\mathbf{x}}))\\
&= \boldsymbol{\phi}\left(\tilde{\mathbf{x}};\psi(\mathbf{x}_1),\dots,\psi(\mathbf{x}_{n_p})\right).
\end{aligned}$$

Thus, the Jacobian for the transformed element is

$$\begin{aligned}
\mathbf{D}\left(\boldsymbol{\phi}(\tilde{\mathbf{x}};\psi(\mathbf{x}_1),\dots,\psi(\mathbf{x}_{n_p}))\right) &= \mathbf{D}\left(\mathbf{A}\boldsymbol{\phi}(\tilde{\mathbf{x}};\mathbf{x}_1,\dots,\mathbf{x}_{n_p})+\mathbf{b}\right)\\
&\overset{\mathbf{b}\text{ is constant}}{=} \mathbf{D}\left(\mathbf{A}\boldsymbol{\phi}(\tilde{\mathbf{x}};\mathbf{x}_1,\dots,\mathbf{x}_{n_p})\right) \qquad (11)\\
&= \mathbf{A}\cdot\mathbf{D}\boldsymbol{\phi}(\tilde{\mathbf{x}};\mathbf{x}_1,\dots,\mathbf{x}_{n_p}).
\end{aligned}$$

Finally, we can prove the invariance of $\hat{\eta}_r$ under ψ:

$$\begin{aligned}
\hat{\eta}_r(\psi(\mathbf{x}_1),\dots,\psi(\mathbf{x}_{n_p})) &= \left(\frac{1}{|t|}\int_t \eta^r(\mathbf{D}\boldsymbol{\phi}(\boldsymbol{\phi}^{-1}(\mathbf{x});\psi(\mathbf{x}_1),\dots,\psi(\mathbf{x}_{n_p})))\,\mathrm{d}\mathbf{x}\right)^{\frac{1}{r}}\\
&\overset{\text{by Eq. (11)}}{=} \left(\frac{1}{|t|}\int_t \eta^r(\mathbf{A}\cdot\mathbf{D}\boldsymbol{\phi}(\boldsymbol{\phi}^{-1}(\mathbf{x});\mathbf{x}_1,\dots,\mathbf{x}_{n_p}))\,\mathrm{d}\mathbf{x}\right)^{\frac{1}{r}}\\
&\overset{\eta\text{ is invariant}}{=} \left(\frac{1}{|t|}\int_t \eta^r(\mathbf{D}\boldsymbol{\phi}(\boldsymbol{\phi}^{-1}(\mathbf{x});\mathbf{x}_1,\dots,\mathbf{x}_{n_p}))\,\mathrm{d}\mathbf{x}\right)^{\frac{1}{r}}\\
&= \hat{\eta}_r(\mathbf{x}_1,\dots,\mathbf{x}_{n_p}).\ \square
\end{aligned}$$

Corollary 1. *If a Jacobian based distortion measure for linear elements fulfills any of the following properties:*

- *translation-free,*
- *rotation-free,*
- *scale-free,*
- *symmetry-free,*

then the proposed high-order distortion and quality measures, Definitions 1 and 2, also hold the same properties.

Proof. Since $\hat{q}_r$ is defined as the inverse of $\hat{\eta}_r$, we only have to prove the previous properties for $\hat{\eta}_r$, Equation (9). All the *translations, scalings, rotations, symmetries*, and their compositions are affine mappings. Therefore, by Proposition 1, we have that $\hat{\eta}_r$ inherits the invariance under translation, or scaling, or rotation, or symmetry that η could have. $\square$

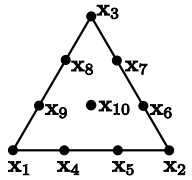

Fig. 2. Mesh composed by a triangle of order three.

Free node	Location 1 (bue)	Location 2 (red)	Location 3 (green)
$\mathbf{x}_3$	$\left(-1, \sqrt{3}/2\right)$	$\left(1/2, \sqrt{3}/2\right)$	$\left(2, \sqrt{3}/2\right)$
$\mathbf{x}_4$	$(1/3, -3/2)$	$(1/3, 0)$	$(1/3, 3/2)$
$\mathbf{x}_{10}$	$(1/2, -1)$	$\left(1/2, \sqrt{3}/6\right)$	$(1/2, 1.5)$

Table 2. Locations of the free node for displacements restricted to one direction.

4 Behavior of the high-order quality measure

In this section we illustrate the behavior of the proposed quality measure for high-order elements. Using Equation (9), we compute the high-order distortion measure for the three algebraic distortion measures presented in Table 1. Then, we use Equation (10) to evaluate the corresponding high-order quality measures. Specifically, we apply three tests to a triangle of order three with nodes located in an equispaced configuration, see Figure 2:

$$\mathbf{x}_1 = (0,0)\,, \quad \mathbf{x}_2 = (1,0)\,, \quad \mathbf{x}_3 = \left(\tfrac{1}{2}, \tfrac{\sqrt{3}}{2}\right), \mathbf{x}_4 = \left(\tfrac{1}{3}, 0\right), \quad \mathbf{x}_5 = \left(\tfrac{2}{3}, 0\right),$$
$$\mathbf{x}_6 = \left(\tfrac{5}{6}, \tfrac{\sqrt{3}}{6}\right), \mathbf{x}_7 = \left(\tfrac{2}{3}, \tfrac{\sqrt{3}}{3}\right), \mathbf{x}_8 = \left(\tfrac{1}{3}, \tfrac{\sqrt{3}}{3}\right), \mathbf{x}_9 = \left(\tfrac{1}{6}, \tfrac{\sqrt{3}}{6}\right), \mathbf{x}_{10} = \left(\tfrac{1}{2}, \tfrac{\sqrt{3}}{6}\right).$$

In each test we consider a free node (keeping the rest of nodes fixed in the equispaced ideal configuration) and compute the quality of the high-order element when the node moves in $\mathbb{R}^2$. The free nodes are: the vertex node $\mathbf{x}_3$, the edge node $\mathbf{x}_4$, and the face node $\mathbf{x}_{10}$. Figure 3 shows the contour plots of the previous high-order qualities for each test.

To visualize the configuration of the high-order triangle and to analyze in more detail the behavior of each high-order quality measure, we now restrict the displacement of the free nodes to one direction: vertex node $\mathbf{x}_3$ moves along the x direction, and edge node $\mathbf{x}_4$ and face node $\mathbf{x}_{10}$ move along the y direction. For each test, Figures 4(a), 4(b) and 4(c) display the configurations of the high order elements corresponding to the location of the free node presented in Table 2.

Figures 4(d), 4(e) and 4(f) plot the three high-order quality measures based on the linear distortion measures presented in Table 1 when:

- vertex node $\mathbf{x}_3 = \left(x_3, \sqrt{3}/2\right)$ moves along the x direction, $x_3 \in [-2, 3]$;
- edge node $\mathbf{x}_4 = (1/3, y_4)$ moves along the y direction, $y_4 \in [-2, 2]$;
- face node $\mathbf{x}_{10} = (1/2, y_{10})$ moves along the y direction, $y_{10} \in [-3/2, 2]$.

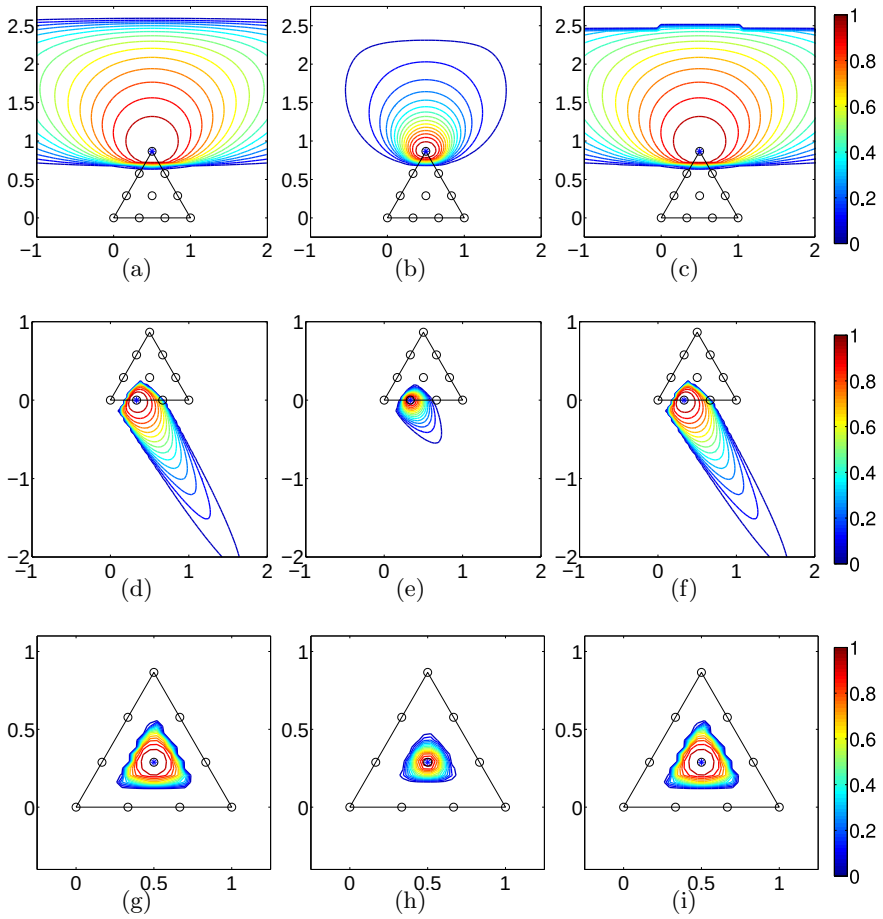

Fig. 3. Level sets for the three high-order quality measures (in columns: shape, Oddy and condition number) when the free node is: (a) to (c) the vertex node $\mathbf{x}_3$; (d) to (f) the edge node $\mathbf{x}_4$; and (g) to (i) the face node $\mathbf{x}_{10}$.

As expected, in Figure 3 we realize that the three high-quality measures have similar behavior. Moreover, all of them define the same feasible region. However, the Oddy high-order quality is more strict and tends to zero faster than the other two measures. In these tests, the high-order quality measure detects all the non-valid configurations. Specifically, it detects tangled elements due to crossed edges or folded areas. Several conclusions can be drawn from Figure 4. From Figures 4(a), 4(b) and 4(c) we realize that moving away a node from its ideal location induces oscillations in the representation of the high-order element, even if the boundary of the element does not change as in Figure 4(c). Hence, tangled elements can appear, see for instance Figures

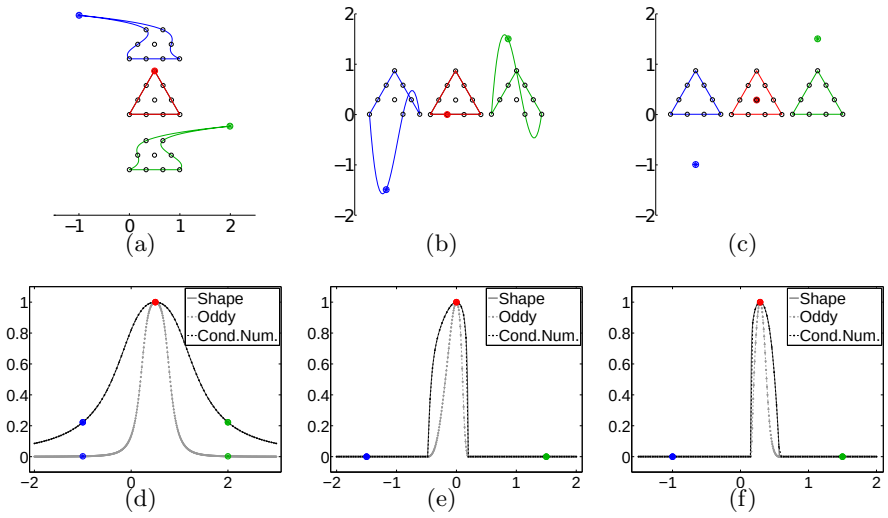

Fig. 4. Configurations and high-order qualities for the three tests. (a) and (b) vertex node $\mathbf{x}_3$ moves on the x direction, (c) and (d) edge node $\mathbf{x}_4$ moves on the y direction; and (e) and (f) face node $\mathbf{x}_{10}$ moves on the y direction.

4(b) and 4(c). From Figures 4(d), 4(e) and 4(f) we first realize that the defined measure properly detects when the high-order element folds and gets tangled. In Figures 4(e) and 4(f) all the measures detect the same tangling positions, where the quality achieves the zero value. Moreover, in all cases, the three measures detect the proper ideal configurations, with quality equals to 1. Note that in Figure 4(d), the three high-order quality measures do not degenerate, despite the Oddy measure decreases faster than the other two. Finally, Figures 3 and 4 show that vertex nodes have larger feasible regions than edge or face nodes.

5 Application to high-order mesh optimization

One of the main problems in high-order mesh generation is to ensure that all the mesh elements are valid (untangled) and regular (smooth). Similarly to the methods proposed for linear meshes [21, 22], we propose to untangle and smooth a high-order mesh by minimizing the distortion of the elements, Definition 1. In this way, we are maximizing the mesh quality since the distortion is the inverse of the quality, Definition 2. For a free node $\mathbf{x}_0$, we define the local value of the objective function as the integral of the distortion measure on all the elements that contain $\mathbf{x}_0$:

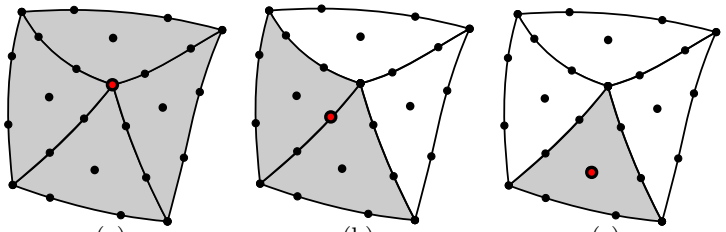

Fig. 5. Local patch for the element-based objective function for a node on: (a) a vertex node, (b) an edge, and (c) a face.

$$f(\mathbf{x}_0) := \left(\frac{1}{\sum_{i=1}^{N} |t_i|} \sum_{i=1}^{N} \int_{t_i} \eta^r \left(\mathbf{D}\boldsymbol{\phi}_i(\boldsymbol{\phi}^{-1}(\mathbf{x})) \right) \mathrm{d}\mathbf{x} \right)^{1/r} \tag{12}$$

where N is the number of elements t_i that contain $\mathbf{x}_0$. Recall that $\boldsymbol{\phi}_i(\tilde{\mathbf{x}}) \equiv \boldsymbol{\phi}_i(\tilde{\mathbf{x}}; \mathbf{x}_1^i, \ldots, \mathbf{x}_0, \ldots, \mathbf{x}_{n_p}^i)$ denotes the mapping between the ideal triangle t_I, and the physical triangle t_i, with nodes $\mathbf{x}_1^i, \ldots, \mathbf{x}_0, \ldots, \mathbf{x}_{n_p}^i$. For all the results presented in this work, we set the value of r to 2. Note that the number of neighboring elements N depends on the position of the node inside the element. That is, if the node is on: a vertex, an edge or a face. In Figure 5 we illustrate the local patch (grey region) around a free node (red circle) depending on its location inside the element.

Finally, to minimize the objective function we perform a local non-linear minimization with updates. This approach is similar to the Gauss-Seidel technique for solving linear systems. Specifically, we loop on all the nodes that are not on the boundary of the mesh. Then, in each step we move the position of one node, and we fix the other ones. To this end, we minimize the local objective function of the node and we update the node location to the optimum. Then, we repeat the process again for the next node.

6 Numerical examples

In this section we apply a high-order quality measure to untangle and smooth non-valid high-order meshes. To this end, we use a high-order distortion based on the shape measure, see Table 1. The initial high-order meshes, and therefore the initial curved boundary approximation, have been computed using the ez4u meshing environment [26, 27, 28]. Mesh quality statistics for the examples are presented in Table 3.

Circular ring. In the first example we generate four meshes of orders 3, 4, 5 and 10 for a circular ring, see Figure 6. The four meshes are composed by 24 elements. The number of nodes depends on the selected order: 126 nodes for order 3, 216 nodes for order 4, 330 nodes for order 5, and 1260 nodes

for order 10. All the initial meshes have the same straight inner edges and only differ on the degree of the polynomial approximation of the boundary. Figure 6(a) shows the initial mesh for order 3 displaying also the quality of its elements. Note that the inner edges of this mesh are straight. Therefore, several tangled elements appear at the inner boundary. Figure 6(b) shows a detail of the upper-right inner boundary of this initial mesh, where a tangled element with null quality appears. It also displays an equispaced sub-grid (in gray) inside each element to visualize the distortion of the mapping between the reference element and the physical one.

Figure 6 shows the initial non-valid meshes and the final optimized meshes. To perform the optimization, we use an equidistributed set of points on the reference and ideal element. In this way, we can plot a straight-sided structured grid on the reference element and map it to the physical element. This sub-grid helps to visualize the behavior of the isoparametric mapping. However, it is well known that for equidistributed interpolation points the Lebesgue constant grows with the interpolation degree. Therefore, the minimum quality for $p = 10$ is slightly worse than for lower degrees, see Table 3. To amend this issue, the interpolation points have to be placed to improve the value the Lebesgue constant. To this end, in practical applications we use an approximated Fekete distribution on both the reference and ideal element. For instance, we use these point distribution in the following example.

Barcelona harbor. In this example we generate a high-order mesh for computing the wave agitation inside the Barcelona (Spain) harbor. The physical problem that is studied is the wave propagation in highly reflective coastal areas. The final goal is to obtain the wave amplification factor for an incident wave of height one. The Barcelona harbor contains several small geometric features (10 m length) compared to the total extension of the domain (12 km), requiring fine computational meshes if linear elements are used. On top of that, high-order elements are needed in order to reduce the numerical dispersion error, commonly associated with the propagation of high frequency waves in presence of numerous reflections. Using a mesh composed by 2.4 millions of linear elements an erroneous solution without physical meaning is obtained. However, using a high-order mesh of order 7 composed by 32802 elements (803649 nodes), the dispersion error can be reduced obtaining an accurate solution. Figure 7 shows the wave amplification factor for the Barcelona harbor when the angle between the incident wave and the x-axis is 43 degrees and the period is 6 seconds [29].

To generate a high-order mesh for this problem, and analogously to the previous example, we first create a triangular mesh composed by elements with curved edges on the boundary of the domain and with straight edges in the interior. Figure 8 shows the initial and smoothed meshes, displaying also the high-order quality of the elements, for the four areas marked in Figure 7. We apply the optimization procedure using a Fekete distribution of nodes on the reference and ideal element. Figures 8(a) to 8(d) present the four selected details of the initial mesh. Note that the three first details contain non-valid

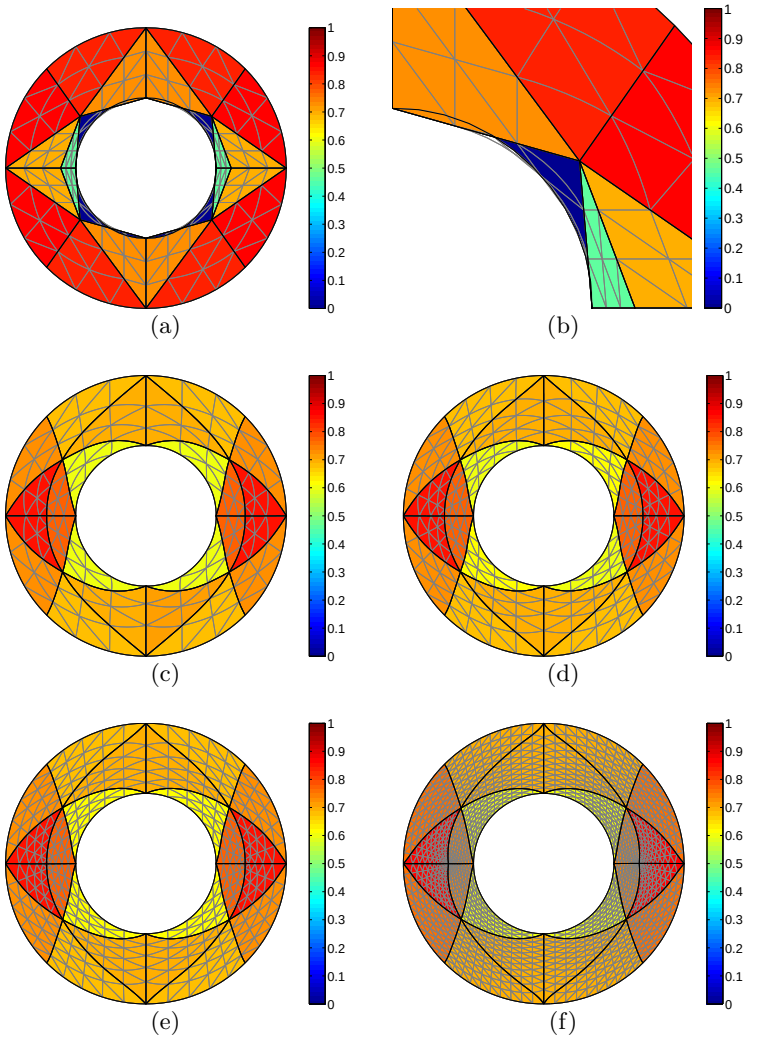

Fig. 6. High-order meshes for the ring: (a) and (b) the initial mesh ($p = 3$); and smoothed and untangled meshes for (c) $p = 3$, (d) $p = 4$, (e) $p = 5$, and (f) $p = 10$.

elements. Figures 8(e) to 8(h) show the four selected details of the smoothed mesh. The final mesh is composed by valid and high-quality elements. Specifically, on the boundary we obtain well shaped elements with curved edges, whereas inner elements tend to have straight edges.

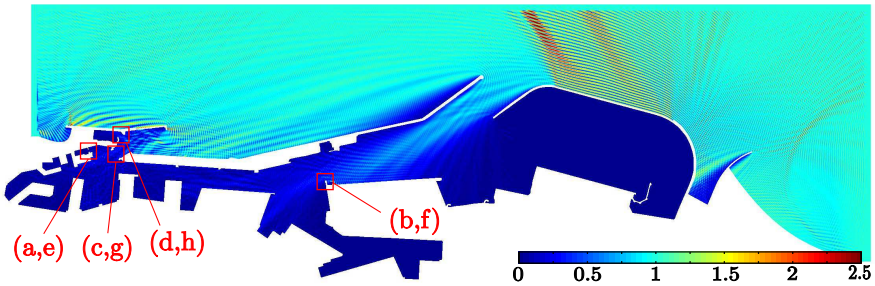

Fig. 7. Wave amplification factor on the Barcelona harbor for an incident wave of height equal to 1 [29]. The solution is obtained on a high-order mesh of order 7.

Meshes	p	Min.	Max.	Mean	Std. dev.	#inv	N_f	N_e	N_v
Initial ring	3	0.00	0.87	0.60	0.31	4	24	84	18
Smoothed ring	3	0.61	0.85	0.72	0.08	0	24	84	18
Smoothed ring	4	0.61	0.85	0.72	0.08	0	72	126	18
Smoothed ring	5	0.61	0.85	0.72	0.08	0	144	168	18
Smoothed ring	10	0.59	0.87	0.72	0.08	0	864	378	18
Initial harbor	7	0.00	1.00	0.91	0.08	3	492030	295218	16401
Smoothed harbor	7	0.36	1.00	0.91	0.02	0	492030	295218	16401

Table 3. High-order quality statistics for the circular ring and the Barcelona harbor: interpolation order (p); minimum, maximum, mean and standard deviation of the quality; number of inverted elements (#inv); and number of inner nodes on faces (N_f), edges (N_e) and vertices (N_v).

7 Concluding remarks and future work

In this work we have presented a technique to define quality measures for nodal high-order triangular elements of any interpolation degree. The quality allows the generalization of quality measures for linear triangles that are based on the Jacobian of an affine mapping. In addition, the generalization inherits the properties of the linear quality measure such as being: invariant under translation, scaling and orthogonal transformations. To assess the reliability of the technique, we have extended and tested three quality measures for linear triangles. The tests show that the obtained high-order quality measures detect invalid and low-quality configurations. Finally, we have shown the applicability of the proposed method by developing a technique to optimize high-order triangular meshes. This technique repairs non-valid elements (untangles) and improves low-quality elements (smooths). The numerical examples show optimized meshes that are fully untangled and composed by higher quality elements. Thus, we can generate high-order triangular meshes that are valid for a finite element simulation on a curved domain. To show this claim, we have included a high-fidelity solution of the Berkhoff equation on a curved mesh of the Barcelona harbor. The curved triangular mesh has been optimized with the proposed technique.

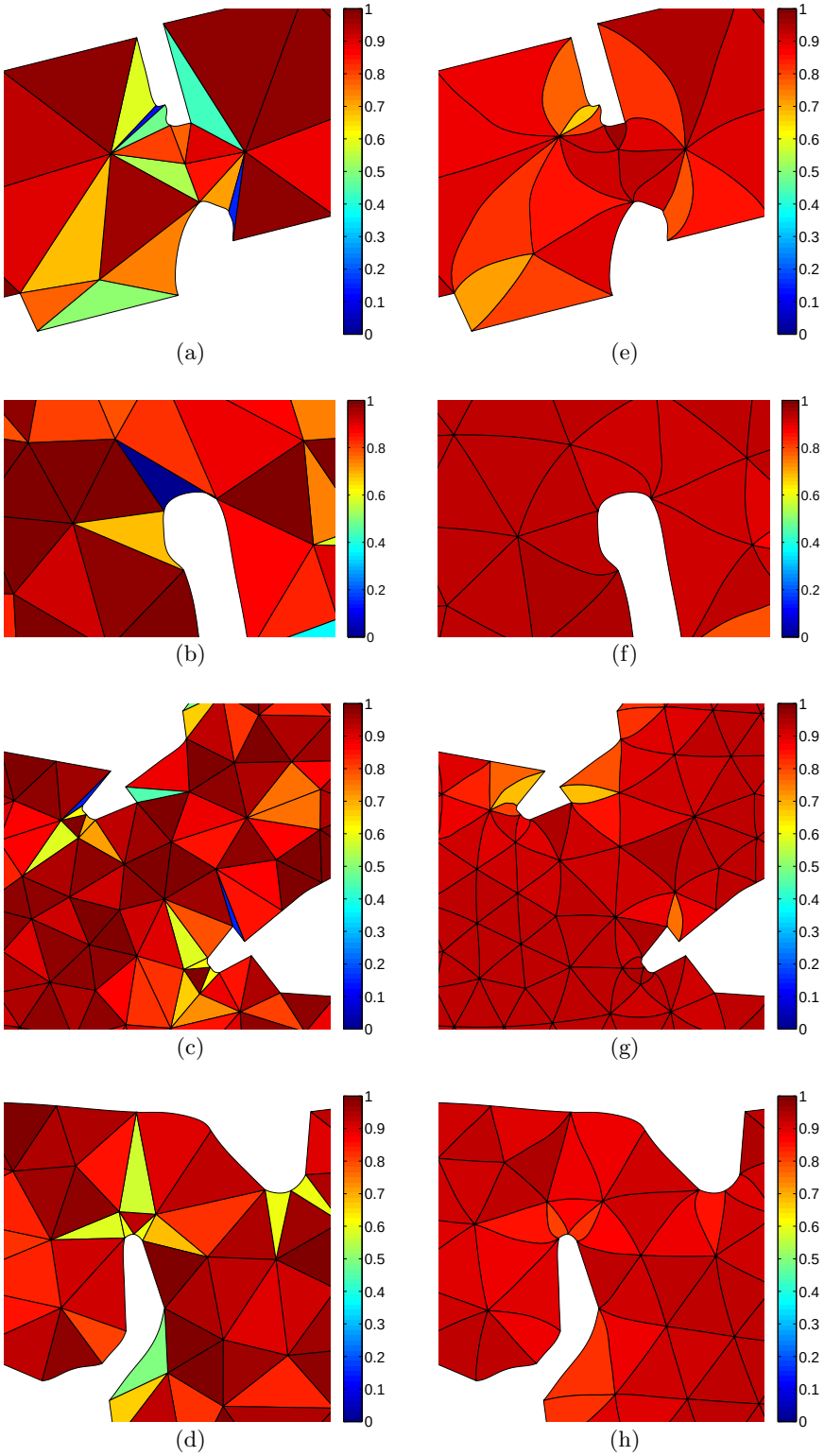

Fig. 8. Details of a high-order mesh for the Barcelona harbour: (a) to (d) details of the initial mesh, (e) to (h) details of the smoothed mesh.

Our long term goal is to develop a mesh optimization tool that untangles and smoothes high-order meshes in 2D and 3D. In this sense, this work presents several limitations that should be investigated and solved in the near future. First, we have only presented quality measures for high-order triangles. Thus, we would like to extend the proposed technique to define quality measures for high-order quadrilaterals, tetrahedra and hexahedra. Second, we have used only the shape quality metric to optimize high-order triangular meshes. Therefore, we would like to compare the results obtained with several quality measures. Third, detailing the implementation of our optimization technique was out of the scope of this paper. However, we would like to detail the formulation and implementation of our procedure in a future work. Finally, in this work we have only ensured local invertibility. Thus, further research is needed to determine the conditions on the coordinates of nodes that ensure global invertibility. To this end, we would like to extend to high-order elements the conditions currently stated only for quadratic elements.

References

1. J Shewchuk. What is a good linear finite element? interpolation, conditioning, anisotropy, and quality measures (preprint). *Preprint*, 2002.
2. S. Dey, M Shephard, and J Flaherty. Geometry representation issues associated with p-version finite element computations. *Comput Method Appl M*, 150(1–4):39–55, 1997.
3. S. Dey, R O'Bara, and M Shephard. Curvilinear mesh generation in 3d. *Comput Aided Design*, 33:199–209, 2001.
4. X Luo, M Shephard, J Remacle, R O'Bara, M Beall, B Szabó, and R. Actis. P-version mesh generation issues. In *11th IMR*, pages 343–354. Citeseer, 2002.
5. X Luo, M Shephard, R O'Bara, R Nastasia, and M Beall. Automatic p-version mesh generation for curved domains. *Eng Comput*, 20(3):273–285, 2004.
6. M Shephard, J Flaherty, K Jansen, X Li, X Luo, N. Chevaugeon, J Remacle, M Beall, and R O'Bara. Adaptive mesh generation for curved domains. *Appl Numer Math*, 52(2-3):251–271, 2005.
7. P Persson and J Peraire. Curved mesh generation and mesh refinement using lagrangian solid mechanics. In *AIAA Proceedings*, 2009.
8. K.Y. Yuan, Y Huang, and T Pian. Inverse mapping and distortion measures for quadrilaterals with curved boundaries. *Int J Numer Meth Eng*, 37(5):861–875, 1994.
9. Z. Chen, J Tristano, and W Kwok. Combined laplacian and optimization-based smoothing for quadratic mixed surface meshes. In *12th IMR*, 2003.
10. L. Branets and G. Carey. Extension of a mesh quality metric for elements with a curved boundary edge or surface. *J Comput Inf Sci Eng*, 5(4):302–308, 2005.
11. A Salem, S. Canann, and S Saigal. Robust distortion metric for quadratic triangular 2d finite elements. *Appl Mech Div ASME*, 220:73–80, 1997.
12. A Salem, S. Canann, and S Saigal. Mid-node admissible spaces for quadratic triangular arbitrarily curved 2d finite elements. *Int J Numer Meth Eng*, 50(2):253–272, 2001.

13. A Salem, S Saigal, and S. Canann. Mid-node admissible space for 3d quadratic tetrahedral finite elements. *Eng Comput*, 17(1):39–54, 2001.
14. P Knupp. Label-invariant mesh quality metrics. In *18th IMR*, 2009.
15. A Mitchell, G Phillips, and E Wachspress. Forbidden shapes in the finite element method. *IMA J Appl Math*, 8(2):260, 1971.
16. D Field. Algorithms for determining invertible two-and three-dimensional quadratic isoparametric finite element transformations. *Int J Numer Meth Eng*, 19(6):789–802, 1983.
17. M Baart and E Mulder. A note on invertible two-dimensional quadratic finite element transformations. *Commun Appl Numer M*, 3(6):535–539, 1987.
18. C de la Vallée Poussin. *Cours d'analyse infinitésimale*, volume 1. Gauthier-Villars, 1921.
19. M Baart and R McLeod. Quadratic transformations of triangular finite elements in two dimensions. *IMA J Numer Anal*, 6(4):475, 1986.
20. A Frey, C Hall, and T Porsching. Some results on the global inversion of bilinear and quadratic isoparametric finite element transformations. *Math Comput*, 32(143):725–749, 1978.
21. P Knupp. A method for hexahedral mesh shape optimization. *Int J Numer Meth Eng*, 58(2):319–332, 2003.
22. J Escobar, E Rodríguez, R Montenegro, G Montero, and J. González-Yuste. Simultaneous untangling and smoothing of tetrahedral meshes. *Comput Method Appl M*, 192(25):2775–2787, 2003.
23. P Knupp. Algebraic mesh quality metrics. *SIAM J Sci Comput*, 23(1):193–218, 2002.
24. P Knupp. Algebraic mesh quality metrics for unstructured initial meshes. *Finite Elem Anal Des*, 39(3):217–241, 2003.
25. S Wandzurat and H Xiao. Symmetric quadrature rules on a triangle. *Comput Math Appl*, 45(12):1829–1840, 2003.
26. X Roca, E Ruiz-Gironés, and J Sarrate. ez4u: Mesh generation environment. `http://www-lacan.upc.edu/ez4u.htm`, 2010.
27. X Roca, J Sarrate, and E Ruiz-Gironés. A graphical modeling and mesh generation environment for simulations based on boundary representation data. In *CMNE*, 2007.
28. X Roca. *Paving the path towards automatic hexahedral mesh generation*. PhD thesis, Universitat Politècnica de Catalunya, 2009.
29. A Huerta, G Giorgiani, and D Modesto. Adaptive cdg and hdg computations. In *16th FEF*, 2011.